EDGE ARTICLE

Check for updates

A mitochondrial-targeted prodrug for NIR imaging guided and synergetic NIR photodynamic-chemo cancer therapy†

Hong-Wen Liu, [ID] ‡[ac] Xiao-Xiao Hu,‡[a] Ke Li,[a] Yongchao Liu,[a] Qiming Rong,[a] Longmin Zhu,[a] Lin Yuan, [ID] [a] Feng-Li Qu, [ID] *[b] Xiao-Bing Zhang [ID] *[a] and Weihong Tan [ID] [a]

Nontoxic prodrugs, especially activated by tumor microenvironment, are urgently required for reducing the side effects of cancer therapy. And combination of chemo-photodynamic therapy prodrugs show effectively synergetic therapeutic efficiency, however, this goal has not been achieved in a single molecule. In this work, we developed a mitochondrial-targeted prodrug **PNPS** for near infrared (NIR) fluorescence imaging guided and synergetic chemo-photodynamic precise cancer therapy for the first time. **PNPS** contains a NIR photosensitizer (**NPS**) and an anticancer drug 5′-deoxy-5-fluorouridine (5′-DFUR). These two parts are linked and caged through a bisboronate group, displaying no fluorescence and very low cytotoxicity. In the presence of H_2O_2, the bisboronate group is broken, resulting in activation of **NPS** for NIR photodynamic therapy and activation of 5′-DFUR for chemotherapy. The activated **NPS** can also provide a NIR fluorescence signal for monitoring the release of activated drug. Taking advantage of the high H_2O_2 concentration in cancer cells, **PNPS** exhibits higher cytotoxicity to cancer cells than normal cells, resulting in lower side effects. In addition, based on its mitochondrial-targeted ability, **PNPS** exhibits enhanced chemotherapy efficiency compare to free 5′-DFUR. It also demonstrated a remarkably improved and synergistic chemo-photodynamic therapeutic effect for cancer cells. Moreover, **PNPS** exhibits excellent tumor microenvironment-activated performance when intravenously injected into tumor-bearing nude mice, as demonstrated by *in vivo* fluorescence imaging. Thus, **PNPS** is a promising prodrug for cancer therapy based on its tumor microenvironment-activated drug release, synergistic therapeutic effect and "turn-on" NIR imaging guide.

Introduction

Significant advances in cancer diagnosis and therapy have been made in the past years, but there still remain several barriers for improving effectiveness and avoiding severe side effects.[1–5] This highlights the need to develop anticancer agents for effectively and selectively killing tumor cells without affecting normal tissues. Photodynamic therapy (PDT), driven by activating photosensitizers (PSs) to generate reactive oxygen species (ROS),

generally singlet oxygen for cancer cell killing, is considered to be a safe, minimally invasive treatment.[6,7] Highly selective photosensitizers are still desirable for accurately localizing and activatable prodrug to minimize side effects and realize more efficient therapeutic outcome. Recently, some activatable PSs have been developed for further minimizing the side effects of PDT.[8,9] The design strategy is generally based on the concept that the prequenched fluorescence and inhibited phototoxicity of the PS which can be restored once a specific trigger is able to separate the quencher or energy acceptor from the vicinity of the PS.[10,11] Moreover, the near infrared (NIR) PSs are desired for PDT, because NIR photons can deeply penetrate the skin and underlying tissue with low damage to the biological samples and minimal background interference.[12–14] Therefore, it's very significant to develop activatable NIR PSs. On the other hand, chemotherapy is one of the most important modalities of cancer treatment. 5-Fluorouracil (5-FUra) has been used in the treatment of a variety of neoplastic diseases. 5′-Deoxy-5-fluorouridine (5′-DFUR), a prodrug of 5-FUra, can be converted to 5-FUra by the thymidine phosphorylase, which is more abundant in tumors than in normal tissues except for the liver

[a]*Molecular Science and Biomedicine Laboratory, State Key Laboratory of Chemo/Biosensing and Chemometrics, College of Chemistry and Chemical Engineering, College of Life Sciences, Aptamer Engineering Center of Hunan Province, Hunan University, Changsha, 410082, P. R. China. E-mail: xbzhang@hnu.edu.cn*

[b]*The Key Laboratory of Life-Organic Analysis, College of Chemistry and Chemical Engineering, Qufu Normal University, Qufu, Shandong, 273165, P. R. China*

[c]*Key Laboratory of Environmentally Friendly Chemistry and Applications of Ministry of Education, College of Chemistry, XiangtanUniversity, Xiangtan 411105, P. R. China*

† Electronic supplementary information (ESI) available. See DOI: 10.1039/c7sc03454g

‡ These authors contributed equally to this work.

of humans.[15] The combination of PDT and chemotherapy with different therapeutic mechanisms has also been proved effective in improving the therapeutic efficiency,[16] which has been achieved mainly *via* co-encapsulated an anticancer drug and a PS in nanocarriers.[17,18] In addition, since the extremely short half-life (<40 ns) and small radius of action (<20 nm) of singlet oxygen ($^1O_2$) in biological systems,[19] direct delivering of PS to hypersensitive subcellular organelles will greatly enhance the PDT efficiency.[20–22] Mitochondria are vital intracellular organelles that play valuable roles in energy production, ROS generation, cellular signalling and regulate apoptosis. Owing to the essential and fatal role of mitochondria, several mitochondrial-targeted anti-cancer drugs have been developed to expect optimal therapeutic efficiency.[23,24] Many evidences also indicate that the damage of mitochondria is the main pathway for PDT-treated cell apoptosis.[20] Thus, mitochondrion is the ideal subcellular target for cancer therapy.

The design of molecular fluorescent probe provides the strategy for developing theranostic prodrugs for targeted and image-guided combination cancer therapy.[25] Fluorescent imaging can provide realtime informations about where, when, and how the prodrugs are delivered and activated *in vivo*.[26] Generally, in such theranostic systems, masked anticancer drugs and imaging reagents are conjugated by tumor-sensitive linkers.[27] Once in the tumor microenvironments, the tumor-sensitive linkers can be broken by tumor over express species, such as low pH,[28] high reactive oxygen species level (including H_2O_2),[29–31] high expressed enzymes,[32–34] and high glutathione (GSH) concentration,[26,35–38] resulting in the release of the anticancer drugs and the activation of the imaging reagents. However, most of previous theranostic drugs do not realize combination of PDT and chemotherapy in a single molecule, which encouraged us to explore molecular theranostic probes with multi-function, including NIR PDT, chemotherapy, subcellular targeting and NIR fluorescence for real-time monitoring the therapeutic effect.

In this work, we developed a mitochondrial-targeted prodrug **PNPS** for NIR fluorescence imaging guided and synergetic chemo-photodynamic precise cancer therapy for the first time. **PNPS** is composed of two moieties and a specific recognition linker as shown in Scheme 1. The first moiety is a NIR fluorescent monitor **NPS**, of which its essential properties of NIR fluorescence and phototoxicity can be countered, yes reversed, by caging its hydroxyl group, act as a prodrug for PDT. Meanwhile, this **NPS** is preferably localized in mitochondria, due to its lipophilic quaternary ammonium salt structure.[39] The second component is an anticancer drug 5′-DFUR. The former two parts are linked and caged through a H_2O_2-sensitive bis-boronate group, displaying no flourescence signal and therapeutic effect. In the presence of H_2O_2, the bisboronate group is broken, resulting in releasing the free **NPS** for NIR PDT and free 5′-DFUR for chemotherapy. The activated **NPS** can also provide a NIR fluorescence signal for monitoring the release of the activated drugs. Taking advantages of the high H_2O_2 concentration in cancer cells, **PNPS** exhibited higher cytotoxicity to cancer cells than normal cells, resulting in lower side effects. In addition, based on its mitochondrial-targeted ability, **PNPS**
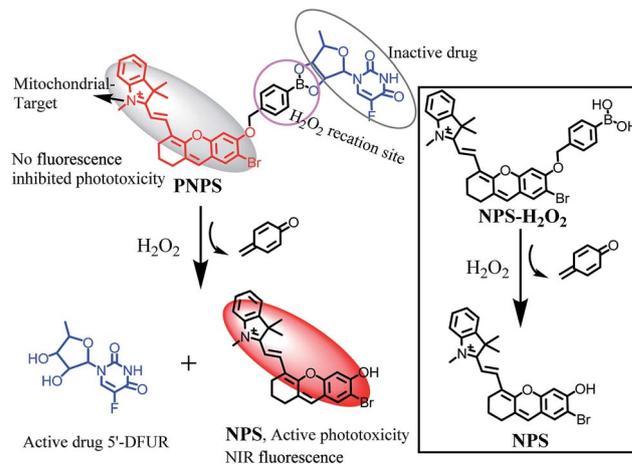
Scheme 1 Design of theranostic prodrug **PNPS** and proposed activation mechanism.

exhibited enhanced chemotherapy efficiency compare to free 5′-DFUR. Moreover, effective chemo-photodynamic combined therapy effects in cancer cells was observed. The *in vitro* and *in vivo* prodrug release was visualized by *in situ* generated NIR fluorescence. These favorable features of tumor microenvironment-activated ability, effective synergistic thertic effect and NIR fluorescence monitoring of the drug release make **PNPS** a promising prodrug.

Results and discussion

We first developed a novel NIR photosensitizer **NPS**, which shows the maximum excitation and emission wavelength at 680 nm and 710 nm, respectively. Since activatable photosensitizers share similar activation mechanisms with activatable fluorophores, the inherent fluorescence of **NPS** is prohibited accompany with inhibited phototoxicity, when the hydroxyl group of **NPS** is caged. Based on the molecular probe design strategy, we hypothesized to develop a subcellular targeted molecular theranostic prodrug with multi-function, such as fluorescence imaging, PDT, chemotherapy, and real-time monitoring of the therapeutic effect. H_2O_2 was chosen as the target for its high sensitivity and specificity toward the boronate moiety and intrinsic enhancement of H_2O_2 levels inside the tumor cell.[40] It was easy to obtain prodrug **NPS-H_2O_2** by attaching the H_2O_2 recognition group (benzoboric acid) to the hydroxyl group of **NPS**. And then, taking the advantage of the reaction between benzoboric acid and pinacol (5′-DFUR contains pinacol group), we obtained the final theranostic prodrug **PNPS**. The synthetic route for **PNPS** was depicted in Fig. S1.† And characterizations of all the new compounds are described in the ESI in detail.†

To verify that H_2O_2 was able to cleave the boronate moiety of prodrug **PNPS** and consequently activate the NIR fluorophore, a chemical transformation experiment of **PNPS** was performed in the presence of H_2O_2 under physiological conditions and monitored by UV-vis and fluorescence spectroscopy. In the UV-vis spectrum as shown in Fig. 1A, **PNPS** showed a strong
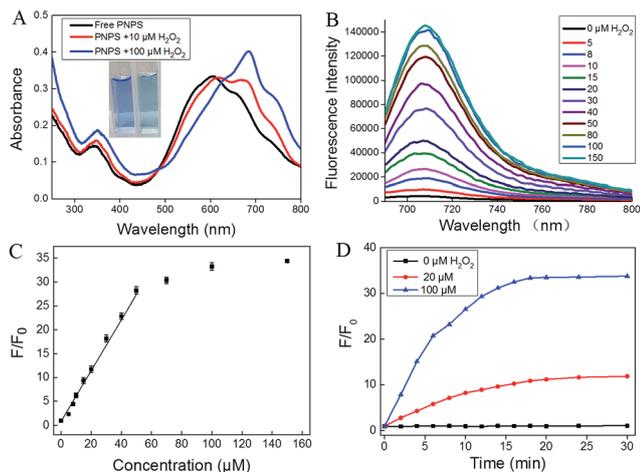
Fig. 1 (A) Absorption and (B) fluorescence emission spectra of PNPS (5 μM) with different concentration H_2O_2 in aqueous solution (PBS/DMSO = 19 : 1, v/v, 10 mM, pH = 7.4). Inset (A) photos of PNPS solution before (left) and after (right) addition of H_2O_2. (C) Calibration curve of PNPS to H_2O_2, the curve was plotted with the fluorescence intensity at 710 nm vs. H_2O_2 concentration. (D) A plot of fluorescence intensity at 710 nm of PNPS vs. the reaction time in the presence of varied concentrations of H_2O_2. λ_{ex} = 680 nm.

absorption peak at λ_{max} = 600 nm. The absorption peak showed a red shift after addition of 100 μM H_2O_2, accompanied by a distinct color change from blue to blue-green (Fig. 1A insert). As shown in Fig. 1B, PNPS exhibited weak fluorescence centered at 710 nm, and gradual addition of H_2O_2 up to 0–150 μM to a solution of PNPS induced the increase of fluorescence intensity. The fluorescence intensity at 710 nm increased by 34.3-fold upon reaction with 150 μM H_2O_2 for 30 min (Fig. 1C). Meanwhile, its intensity increased linearly with the concentration of H_2O_2 ranging from 5 to 40 μM (Fig. S2†). The catalytic efficiency of H_2O_2 toward the PNPS was assessed. Fluorescence kinetic curves of H_2O_2 at varied concentrations (0, 20, 100 μM) reacting with PNPS were depicted in Fig. 1D. As was shown, a higher concentration of H_2O_2 could induce faster cleavage reaction and therefore result in increased fluorescence intensity. The fluorescence signal of the reaction system could reach a plateau in about 20 min. Meanwhile, in the absence of H_2O_2, testing the generation of a false positive signal by spontaneous hydrolysis, gave no detectable signal increase, even over 12 h (Fig. S3†), demonstrating that PNPS was stable in the reaction system. These results demonstrated that after reaction with H_2O_2, PNPS was efficiently activated and the released NPS could provide a turn-on NIR fluorescence signal for drug release and therapeutic efficacy monitoring.

The selectivity of prodrug PNPS for H_2O_2 over other biologically relevant ROS species, metal ions, amino acids and proteins was evaluated. As shown in Fig. S4A,† no significant changes in fluorescence intensity were observed upon addition of the other ROS species, metal ions, amino acids and proteins to prodrug PNPS. The pH effect on the H_2O_2-induced fluorescence changes of PNPS was also investigated. As shown in Fig. S4B,† PNPS remained stable and emitted a weak fluorescence within 4.0–9.0 pH range. After treatment by 25 μM of

H_2O_2, the fluorescence at 710 nm was activated and reached saturation in the 7.4–8.0 pH range. The above results indicated that prodrug PNPS can be applied as a H_2O_2-activated theranostic prodrug under physiological pH condition with high selectivity.

To confirm the fluorescence response mechanism, the reaction products of PNPS with H_2O_2 were analyzed by HPLC and HRMS. As illustrated in Fig. S5,† pure PNPS showed a unique peak with retention time at about 5.36 min, and compound NPS exhibited a peak at about 6.25 min. After PNPS incubation with H_2O_2 for 30 min, a new peak at 6.25 min corresponding to compound NPS was clearly observed, and the peak corresponding to PNPS was sharply decreased. Moreover, in the ESI-HRMS (positive ion mode) spectrum of PNPS incubated with H_2O_2 for 30 min, the peaks of NPS and 5′-DFUR were found at m/z 464.1065 and 269.0462 respectively (Fig. S6†). These results demonstrated that the H_2O_2 cleaved recognition site, then PNPS was activated and free NPS and 5′-DFUR were released.

On the basis of the positive results showing H_2O_2-activated release of active drug and concurrent fluorescence enhancement, PNPS was next tested in cultured cells. Cellular fluorescence imaging of PNPS were investigated in four different cell lines, HeLa, HepG2, HCT116 and HL7702 cells. HeLa, HepG2 and HCT116 cancer cells were pretreated with prodrug PNPS (5 μM) for different time, then fluorescence imaging were carried out. The increased fluorescence intensity of HeLa, HepG2 and HCT116 cells indicated the efficient activation of theranostic PNPS by endogenous H_2O_2 in the tumor cells without any external inducer (Fig. 2A and S7–S9†). In addition, HeLa cells pretreated with exogenous H_2O_2 for 0.5 h and then incubated with PNPS for another 0.5 h, the fluorescence intensity dramatically increased. The cellular activation of PNPS
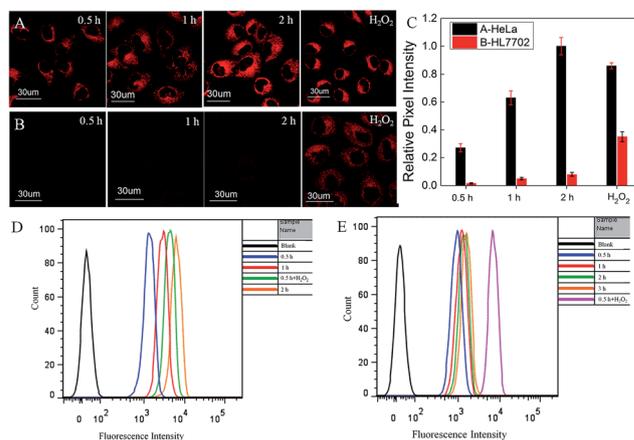

Fig. 2 Cellular fluorescence images of prodrug PNPS-treated HeLa (A) and HL7702 (B) cells. The cells were incubated with PNPS (5 μM) for 0.5 h, 1 h and 2 h, respectively, or the cells were pretreated with H_2O_2 (100 μM) for 0.5 h and then incubated with PNPS for another 0.5 h. (C) Relative pixel intensity (n = 3) from images (A and B). The pixel intensity from image (A) 2 h is defined as 1.0. Flow cytometric analysis of PNPS (5 μM) fluorescence after incubated with HeLa (D) or HL7702 (E) cells for different time; or cells incubated with PNPS for 0.5 h and H_2O_2 (100 μM) for another 0.5 h. λ_{ex} = 635 nm, λ_{em} = 680–750 nm.

were further confirmed by flow cytometry analysis (Fig. 2D). Similar phenomena were also observed in HepG2 cells (Fig. S8†), and the activation performance of **PNPS** in HepG2 after incubated for 2 h is 10% higher than that for HeLa cells calculated from the results of flow cytometry. These results indicated that the oxidation of boronate moiety of theranostic **PNPS** generated fluorescence enhancement, depending upon amount of intracellular H_2O_2, as depicted in Scheme 1. Normal HL-7702 cells were also incubated with prodrug **PNPS** for an examination of the effect of H_2O_2 on the bioactivity of **PNPS**. Very weak fluorescence signals were observed in HL-7702 cells by confocal microscopy after incubating with **PNPS** for 0.5 h, 1 h or 2 h (Fig. 2B). However, after pretreated with 100 μM H_2O_2 for 0.5 h, a strong fluorescent enhancement was observed in HL-7702 cells. The flow cytometry analysis results also confirmed that **PNPS** kept inactivated in HL-7702 cells (Fig. 2E). These results demonstrated that prodrug **PNPS** showed cancer cells-targeted activated ability.

Furthermore, mitochondrial localization of activated prodrug **PNPS** was investigated by colocalization experiments using a commercialized mitochondria fluorescent tracker, Mitotracker Green. As shown in Fig. 3 and S10,† the fluorescence signal that was ascribed to **PNPS** colocalized well with the Mitotracker (Pearson's correlation factor is 0.965, 0.943 and 0.958 for HeLa cells, HepG2 cells and HCT116 cells respectively), due to its lipophilic quaternary ammonium salt structure. Further experiments were carried out to demonstrate that most **PNPS** molecules will locate in mitochondria before reaction with cytoplasm H_2O_2, with the results showed in Fig S11.† This is mainly because the **PNPS** molecular can fast diffuse into cells and target mitochondria (within 10 min) before reaction with relatively low concentration cytoplasm H_2O_2. These results demonstrated the outstanding mitochondrial-targeting ability of **PNPS**, which may help improve the therapeutic effect.

The $^1O_2$ generation of **PNPS** in buffer solution in the present of H_2O_2 upon light irradiation was studied using 9, 10-diphenylanthracene (DPHA)[41] and fluorescent probe MNAH[42] as indicators. DPHA is a $^1O_2$ indicator, whose absorbance decreases upon interaction with $^1O_2$. In the presence of H_2O_2, when incubating DPHA with **PNPS** upon white light irradiation, the absorbance of DPHA decreased gradually (Fig. S12A†). Meanwhile, pretreated **PNPS** with H_2O_2 and then incubated with fluorescent probe MNAH upon white light irradiation, the fluorescence of MNAH increased gradually (Fig. S13A†). But in

the absence of H_2O_2, the absorbance of DPHA or the fluorescence of MNAH showed limited changes (Fig. S12B and S13B†). And the compared results were shown in the Fig. 4A and Fig. 4B, obvious difference could be observed between those whether pretreated with H_2O_2. These results demonstrated that **PNPS** could efficiently generate $^1O_2$ in buffer solution after activated by H_2O_2, indicated its activable phototoxicity. The $^1O_2$ generation of **PNPS** in cells upon light irradiation was studied using 2′,7′-dichlorofluorescin diacetate (DCF-DA) as a cell-permeable probe. DCF-DA is nonfluorescent but can be oxidized by $^1O_2$ to yield highly fluorescent 2′,7′-dichlorofluorescein (DCF). As shown in Fig. 4C, strong green fluorescence could only be observed when the cells were treated with **PNPS** for 2 h followed by light irradiation. The results confirmed the $^1O_2$ generation by activated **PNPS** in live HeLa cells upon light irradiation.

We then investigated the ability of prodrug **PNPS** to selectively target cancer cells by measuring its cytotoxicity to HeLa, HepG2 and HL-7702 cells. MTS assays were used to study cytotoxicity of **PNPS**, **NPS-H_2O_2** and 5′-DFUR under dark. After 3 h incubation, **NPS-H_2O_2** and 5′-DFUR exhibited low cytotoxicity even at a high concentration of 15 μM as more than 80% of the tested HeLa and HepG2 cells survived (Fig. 5). On the contrary, **PNPS** demonstrated much higher dark cytotoxicity with an IC_{50} value of 16.6 μM and 14.8 μM for HeLa cells and HepG2 cells respectively (Fig. S14 and 15†). Taken together, these results illustrated that **PNPS** exhibited enhanced cytotoxicity over commercial 5′-DFUR. For **PNPS**, in addition to the high cytotoxicity under dark conditions, under white light
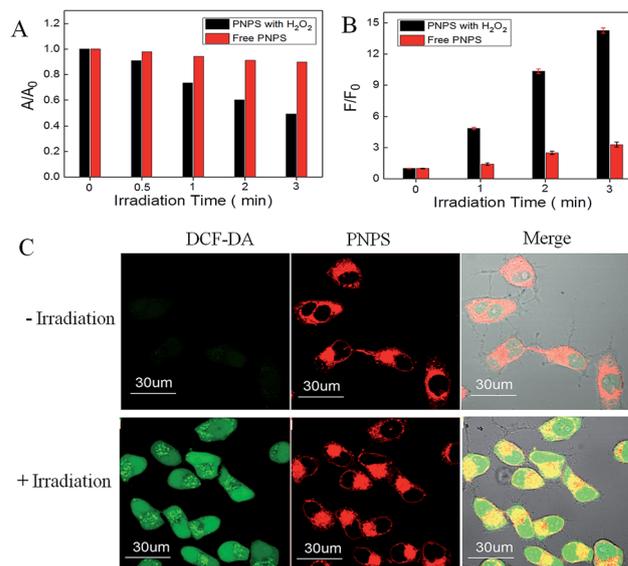

Fig. 4 (A) The change of DPHA absorbance at 373 nm in the presence of **PNPS** after different durations of white light irradiation. (B) The change of MNAH fluorescence intensity at 535 nm in the presence of **PNPS** after different durations of white light irradiation. The blank bar represents the reaction solution pretreated with H_2O_2 for 0.5 h before light irradiation, the red bar represents without H_2O_2 pretreatment. (C) Fluorescence imaging showing the $^1O_2$ generation of **PNPS** (5 μM) in HeLa cells after different treatments using (DCF-DA, 2 μM) as indicator. The green channel is from DCF-DA (ex: 488 nm, em: 500–550 nm); the red channel is from **PNPS** (λ_{ex} = 635 nm, λ_{em} = 680–750 nm).
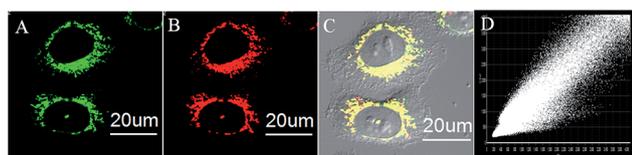

Fig. 3 Fluorescence images of co-localized experiment in HeLa cells. The cells were incubated with **PNPS** for 0.5 h and then incubated with MitoTracker Green for another 0.5 h. (A) MitoTracker Green (0.5 μM, λ_{ex} = 488 nm, λ_{em} = 500–550 nm). (B) Prodrug **PNPS** (5 μM, λ_{ex} = 635 nm, λ_{em} = 680–750 nm). (C) Overlay of (A) and (B). (D) Intensity correlation plot of stain, the Pearson's correlation factor is 0.965.

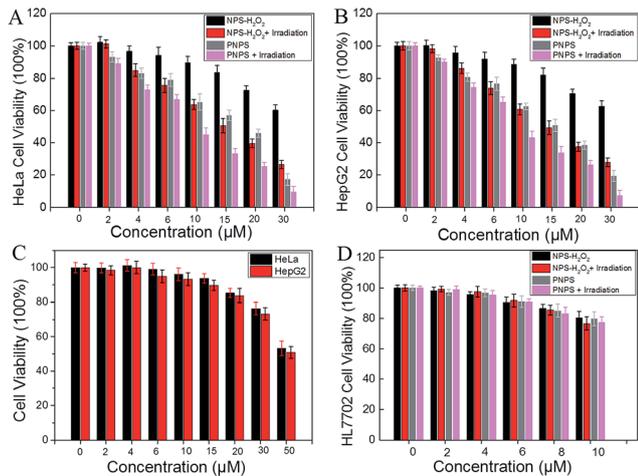Fig. 5 Viability of (A) HeLa, (B) HepG2 and (D) HL7702 cells upon treatment with different concentrations of **NPS-H$_2$O$_2$** or **PNPS** showed under white light irradiation or in dark. (C) Viability of HeLa (black bar) and HepG2 (red bar) cells upon treatment with different concentrations of 5′-DFUR.

illumination, it could generate $^1O_2$ and exhibited high phototoxicity to cancer cells. Notably, under white light illumination, the IC$_{50}$ value of **PNPS** towards HeLa and HepG2 cells was 9.32 μM and 8.15 μM respectively (Fig. S14 and 15†), which was lower than that of **PNPS** without light irradiation (Fig. 5A and B). And compare to **NPS-H$_2$O$_2$**, **PNPS** showed enhanced cytotoxicity to cancer cells, due to its chemo-photodynamic combination therapy. However, both **PNPS** and **NPS-H$_2$O$_2$** showed lower cytotoxicity even at a high concentration of 10 μM towards HL-7702 cells as more than 75% of the tested HL-7702 cells survived (Fig. 5D). As contrast, compound **NPS** exhibited high phototoxicity to HL-7702 cells (Fig. S16†), with IC$_{50}$ value of 8.50 μM (Fig. S17†). These results indicated that the prodrugs **PNPS** and **NPS-H$_2$O$_2$** show low cytotoxicity to normal HL-7702 cells, which may mainly because that **PNPS** and **NPS-H$_2$O$_2$** kept inactivated in HL-7702 cells. Collectively, these results demonstrated that the combination chemo-therapy and PDT provides higher anticancer effect compared to the single therapeutic approach alone.

The propidium iodide (PI) staining experiments were further carried out to demonstrate MTS results. PI, a cell impermeable
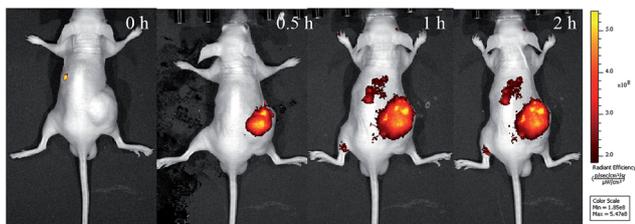

Fig. 6 *In vivo* imaging of HCT116 tumor-bearing mice at various time (0, 0.5, 1 h and 2 h) after orthotopic injection of the prodrug **PNPS** (0.288 mg kg^{-1}). 0 h means that the images was captured immediately after injection.
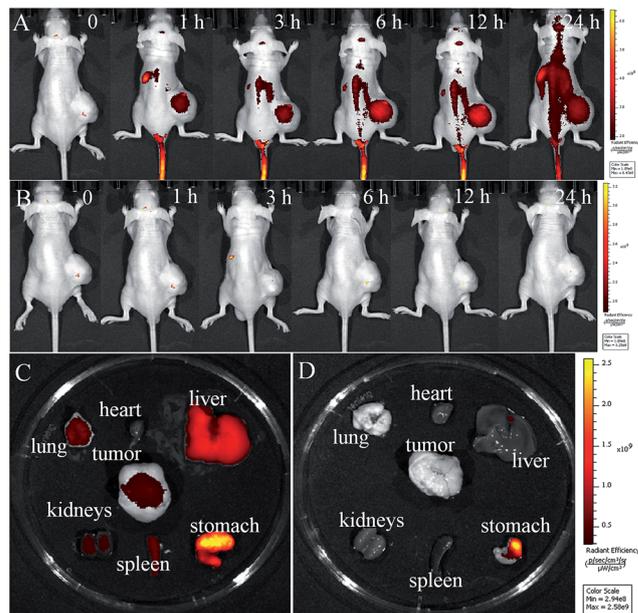

Fig. 7 *In vivo* imaging of HCT116 tumor-bearing mice at various times after intravenous injection of (A) prodrug **PNPS** (4.31 mg kg^{-1}) and (B) saline. Fluorescence images of the internal organs at 25 h post injection after anatomy for prodrug **PNPS** (C) and saline (D). 0 h means that the images was captured immediately after injection.

dye, only stains dead cells or late apoptotic cells with damaged membrane. As shown in Fig. S18,† **PNPS**-treated HeLa cells incubated under the dark was stained whereas nearly all the cells were stained after they were exposed to white light irradiation. Meanwhile, HL-7702 cells were incubated with **PNPS** much fewer cells were stained even after white light irradiation. However, when HL-7702 cells were first treated with H$_2$O$_2$ and follow with **PNPS**, most cells were stained after white light irradiation. Collectively, these results indicate that **PNPS** achieves lower side effects to normal cells.

Benefit from its NIR fluorescence, the activation of the prodrug **PNPS** in tumor-bearing mice could be investigated *via in vivo* fluorescence imaging. The nude mice bearing HCT116 xenografts were injected in the tumor site with the prodrug **PNPS**, and *in vivo* images were obtained at various times. As shown in Fig. 6, NIR fluorescence intensity representing the release of the activated drug, was clearly observed at 0.5 h after the injection of the **PNPS**, the NIR fluorescence then increased in time-dependent manner. These results indicated that theranostic prodrug **PNPS** could be effectively activated in the tumor and could be used for real-time fluorescence monitoring of the therapeutic effect *in vivo*.

We further investigated the activation and bio-distribution of prodrugs **PNPS** with HCT116 tumor-bearing mice, intravenously injected with **PNPS** and saline. As shown in Fig. 7A, the obvious fluorescence was seen in the tumor region after treated by prodrug **PNPS** for 1 h, indicative of the rapid distribution of **PNPS** *via* the blood circulation and the effective activation of **PNPS** in tumor. And a significant fluorescence enhancement was observed in tumor as time continued before 12 h post

injection due to the gradual prodrug activation, and it faded out as time further increased, owing to the excretion of the activated drug. In contrast, negligible signals were obtained in the saline-treated mice (Fig. 7B). And during the distribution process of 12 h, **PNPS** had the strongest fluorescence, representing the largest amount of released drug, in the tumor. These results indicated prominent tumor-targeting activation ability of **PNPS**. The tumor-targeting drug release along with fluorescence enhancement could be ascribed to the particularly high H_2O_2 concentration in cancer cells. Furthermore, in fluorescence images of the internal organs at 25 h post injection after anatomy, an obvious fluorescence was observed in the tumor, liver and stomach of mice treated by prodrug **PNPS**, and much weaker fluorescence were seen in lung, heart, kidney and spleen (Fig. 7C). Meanwhile, in the control experiments, no obvious fluorescence were observed in the tumor or other internal organs (Fig. 7D). The tumor-targeting ability and the specific drug release in tumor make **PNPS** a promising prodrug to achieve high efficacy and reduced side effects.

Conclusions

In summary, by conjugating the anticancer drug 5′-DFUR and NIR photosensitizer (**NPS**) *via* a bisboronate bond, we developed a novel H_2O_2-responsive NIR theranostics prodrug **PNPS**. The phototoxicity and inherent NIR fluorescence of **NPS** and the cytotoxicity of the drug (5′-DFUR) are quenched by the covalent H_2O_2-responsive linker. **PNPS** can be effectively activated by the high concentration of H_2O_2 in cancer cells or in tumor as monitored by the turn-on NIR fluorescence. **PNPS** shows enhanced chemotherapy efficiency compare to free 5′-DFUR due to its mitochondrial-targeting ability. Furthermore, it shows remarkably improved and synergistic chemo-photodynamic therapeutic effect for cancer cells. More importantly, **PNPS** exhibits higher cytotoxicity to cancer cells than that to normal HL-7702 cells, resulting in lower side effects. Therefore, the prodrug **PNPS** provides a promising platform for specific tumor-activatable drug delivery system, which can be easily monitored by cellular and *in vivo* NIR fluorescence imaging. This study also suggests that the molecular probe design strategy, which combines the key functions of targeting, release, imaging, and treatment within a single agent, may play an important role in cancer diagnosis and therapy.

Conflicts of interest

There are no conflicts to declare.

Acknowledgements

Notes and references

1 A. Umar, B. K. Dunn and P. Greenwald, *Nat. Rev. Cancer*, 2012, **12**, 835–848.

2 P. E. Goss and A. F. Chambers, *Nat. Rev. Cancer*, 2010, **10**, 871–877.

3 X. Li, J. Kim, J. Yoon and X. Chen, *Adv. Mater.*, 2017, **29**, 1606857.

4 H. Ju, *Sci. China: Chem.*, 2015, **58**, 438.

5 W. Pan, H. Yang, T. Zhang, Y. Li, N. Li and B. Tang, *Anal. Chem.*, 2013, **85**, 6930–6935.

6 J. P. Celli, B. Q. Spring, I. Rizvi, C. L. Evans, K. S. Samkoe, S. Verma, B. W. Pogue and T. Hasan, *Chem. Rev.*, 2010, **110**, 2795.

7 A. P. Castano, P. Mroz and M. R. Hamblin, *Nat. Rev. Cancer*, 2006, **6**, 535–545.

8 X. S. Li, S. Kolemen, J. Yoon and E. U. Akkaya, *Adv. Funct. Mater.*, 2017, **27**, 1604053.

9 S. Kolemen, M. Isik, G. M. Kim, D. Kim, H. Geng, M. Buyuktemiz, T. Karatas, X. F. Zhang, Y. Dede, J. Yoon and E. U. Akkaya, *Angew. Chem., Int. Ed.*, 2015, **54**, 5340–5344.

10 J. F. Lovell, T. W. B. Liu, J. Chen and G. Zheng, *Chem. Rev.*, 2010, **110**, 2839–2857.

11 R. Musiol, M. Serda and J. Polanski, *Curr. Pharm. Des.*, 2011, **17**, 3548–3559.

12 Z. Guo, S. Park, J. Yoon and I. Shin, *Chem. Soc. Rev.*, 2014, **43**, 16–29.

13 X. Chen, D. Lee, S. Yu, G. Kim, S. Lee, Y. Cho, H. Jeong, K. T. Nam and J. Yoon, *Biomaterials*, 2017, **122**, 130–140.

14 N. Li, Z. Yu, W. Pan, Y. Han, T. Zhang and B. Tang, *Adv. Funct. Mater.*, 2013, **23**, 2255–2262.

15 H. Eda, K. Fujimoto, S.-i. Watanabe, M. Ura, A. Hino, Y. Tanaka, K. Wada and H. Ishitsuka, *Cancer Chemother. Pharmacol.*, 1993, **32**, 333–338.

16 M. Olivo, R. Bhuvaneswari, S. S. Lucky, N. Dendukuri and P. Soo-Ping Thong, *Pharmaceuticals*, 2010, **3**, 1507–1529.

17 W. Zhang, J. Shen, H. Su, G. Mu, J.-H. Sun, C.-P. Tan, X.-J. Liang, L.-N. Ji and Z.-W. Mao, *ACS Appl. Mater. Interfaces*, 2016, **8**, 13332–13340.

18 Y. Zhang, F. Huang, C. Ren, L. Yang, J. Liu, Z. Cheng, L. Chu and J. Liu, *ACS Appl. Mater. Interfaces*, 2017, **9**, 13016–13028.

19 P. R. Ogilby, *Chem. Soc. Rev.*, 2010, **39**, 3181–3209.

20 R. Hilf, *J. Bioenerg. Biomembr.*, 2007, **39**, 85–89.

21 L. Rajendran, H. J. Knolker and K. Simons, *Nat. Rev. Drug Discovery*, 2010, **9**, 29–42.

22 Z. Yu, W. Pan, N. Li and B. Tang, *Chem. Sci.*, 2016, **7**, 4237–4244.

23 S. Fulda, L. Galluzzi and G. Kroemer, *Nat. Rev. Drug Discovery*, 2010, **9**, 447–464.

24 Z. Yu, Q. Sun, W. Pan, N. Li and B. Tang, *ACS Nano*, 2015, **9**, 11064–11074.

25 C.-J. Zhang, Q. Hu, G. Feng, R. Zhang, Y. Yuan, X. Lu and B. Liu, *Chem. Sci.*, 2015, **6**, 4580–4586.

26 M. Z. Ye, X. H. Wang, J. B. Tang, Z. Q. Guo, Y. Q. Shen, H. Tian and W. H. Zhu, *Chem. Sci.*, 2016, **7**, 4958–4965.

27 M. Gao, F. Yu, C. Lv, J. Choo and L. Chen, *Chem. Soc. Rev.*, 2017, **46**, 2237–2271.

28 J.-Z. Du, X.-J. Du, C.-Q. Mao and J. Wang, *J. Am. Chem. Soc.*, 2011, **133**, 17560–17563.

29 Y. Y. Yuan, C. J. Zhang, S. D. Xu and B. Liu, *Chem. Sci.*, 2016, **7**, 1862–1866.

30 E.-J. Kim, S. Bhuniya, H. Lee, H. M. Kim, C. Cheong, S. Maiti, K. S. Hong and J. S. Kim, *J. Am. Chem. Soc.*, 2014, **136**, 13888–13894.

31 R. Kumar, J. Han, H.-J. Lim, W. X. Ren, J.-Y. Lim, J.-H. Kim and J. S. Kim, *J. Am. Chem. Soc.*, 2014, **136**, 17836–17843.

32 Y. Ichikawa, M. Kamiya, F. Obata, M. Miura, T. Terai, T. Komatsu, T. Ueno, K. Hanaoka, T. Nagano and Y. Urano, *Angew. Chem., Int. Ed.*, 2014, **53**, 6772–6775.

33 Y. Y. Yuan, C. J. Zhang, M. Gao, R. Y. Zhang, B. Z. Tang and B. Liu, *Angew. Chem., Int. Ed.*, 2015, **54**, 1780–1786.

34 G. Zheng, J. Chen, K. Stefflova, M. Jarvi, H. Li and B. C. Wilson, *Proc. Natl. Acad. Sci. U. S. A.*, 2007, **104**, 8989–8994.

35 F. P. Kong, Z. Y. Liang, D. R. Luan, X. J. Liu, K. H. Xu and B. Tang, *Anal. Chem.*, 2016, **88**, 6450–6456.

36 X. Wu, X. Sun, Z. Guo, J. Tang, Y. Shen, T. D. James, H. Tian and W. Zhu, *J. Am. Chem. Soc.*, 2014, **136**, 3579–3588.

37 S. Bhuniya, S. Maiti, E. J. Kim, H. Lee, J. L. Sessler, K. S. Hong and J. S. Kim, *Angew. Chem., Int. Ed.*, 2014, **53**, 4469–4474.

38 S. Santra, C. Kaittanis, O. J. Santiesteban and J. M. Perez, *J. Am. Chem. Soc.*, 2011, **133**, 16680–16688.

39 L. Yuan, W. Lin, S. Zhao, W. Gao, B. Chen, L. He and S. Zhu, *J. Am. Chem. Soc.*, 2012, **134**, 13510–13523.

40 E. W. Miller and C. J. Chang, *Curr. Opin. Chem. Biol.*, 2007, **11**, 620–625.

41 Y. Yuan, C.-J. Zhang, S. Xu and B. Liu, *Chem. Sci.*, 2016, **7**, 1862–1866.

42 H.-W. Liu, S. Xu, P. Wang, X.-X. Hu, J. Zhang, L. Yuan, X.-B. Zhang and W. Tan, *Chem. Commun.*, 2016, **52**, 12330–12333.